

# Thermodynamic computing out of equilibrium

Stephen Whitelam<sup>1,\*</sup> and Corneel Casert<sup>1,†</sup>

<sup>1</sup>*Molecular Foundry, Lawrence Berkeley National Laboratory, 1 Cyclotron Road, Berkeley, CA 94720, USA*

We present the design for a thermodynamic computer that can perform arbitrary nonlinear calculations in or out of equilibrium. Simple thermodynamic circuits, fluctuating degrees of freedom in contact with a thermal bath and confined by a quartic potential, display an activity that is a nonlinear function of their input. Such circuits can therefore be regarded as thermodynamic neurons, and can serve as the building blocks of networked structures that act as thermodynamic neural networks, universal function approximators whose operation is powered by thermal fluctuations. We simulate a digital model of a thermodynamic neural network, and show that its parameters can be adjusted by genetic algorithm to perform nonlinear calculations at specified observation times, regardless of whether the system has attained thermal equilibrium. This work expands the field of thermodynamic computing beyond the regime of thermal equilibrium, enabling fully nonlinear computations, analogous to those performed by classical neural networks, at specified observation times.

## I. INTRODUCTION

While classical forms of computing view thermal fluctuations as an obstacle to computation [1–3], thermodynamic computing uses thermal fluctuations as a means of doing computation [4–10]. Fluctuations can drive state changes in devices, and can be used to encode information. For instance, consider scalar degrees of freedom  $x_i$  that interact via the bilinear couplings  $J_{ij}x_ix_j$ . If these degrees of freedom are placed in contact with a thermal bath at temperature  $T$ , then the equilibrium two-point correlations  $\langle x_ix_j \rangle_0 = k_B T (J^{-1})_{ij}$  encode the elements of the matrix inverse of  $J$ . Thus measuring such correlations in equilibrium can be used to do matrix inversion [11, 12].

A major focus of thermodynamic computing is to arrange for the equilibrium properties of a thermodynamic computer, described by the Boltzmann distribution, to correspond to the output of a specified computation. This approach is powerful, because knowing the interaction energy  $U(\mathbf{x})$  of the degrees of freedom  $\mathbf{x}$  of a thermodynamic computer specifies the Boltzmann distribution  $\rho_0(\mathbf{x}) = Z^{-1}e^{-\beta U(\mathbf{x})}$ , where  $\beta^{-1} \equiv k_B T$  and  $Z$  is the partition function. Thus by designing the interactions of the thermodynamic computer we can design its equilibrium properties [11]. However, this approach comes with two challenges. One is that we need the computer to attain thermal equilibrium. In general, physical systems equilibrate on a broad range of timescales [13–16], and the equilibration times for even a simple thermodynamic computer can vary by orders of magnitude as its program is altered [17]. A second challenge is that not every calculation can be represented by the Boltzmann distribution in an obvious way. For example, the matrix inversion described above can only be done if the matrix  $J_{ij}$  is symmetric and positive definite. If it is not

symmetric, we have  $(J^{-1})_{ij} \neq (J^{-1})_{ji}$  in general, but we must have  $\langle x_ix_j \rangle_0 = \langle x_jx_i \rangle_0$ , and so the relation described in the first paragraph cannot hold; if it is not positive definite, the system does not have a well-defined equilibrium distribution.

We can sidestep these challenges by arranging for a thermodynamic computer to perform calculations *out* of equilibrium. Out of equilibrium we lose contact with the theoretical foundation provided by the Boltzmann distribution, and so we must find other ways of programming a thermodynamic computer in order to do specified calculations. Some exceptions to the equilibrium paradigm already exist. For instance, the matrix exponential  $e^{-Jt}$  can be calculated at observation time  $t$  [18], and nonequilibrium work measurements can be used to calculate the determinant of a matrix [11]. However, no design exists for a general-purpose programmable thermodynamic computer that operates at specified observation times. Here we introduce such a design by introducing a thermodynamic computer that is analogous to a neural network. A thermodynamic computer of this nature is a nonlinear model that can serve as a universal function approximator, and can be programmed to perform arbitrary nonlinear computations at specified observation times. This is true whether or not the computer has attained thermodynamic equilibrium at those observation times.

In more detail, we introduce a thermodynamic neuron, a fluctuating classical degree of freedom placed in contact with a heat bath and confined by a quartic potential [19]. The equilibrium average of the neuron activation is a nonlinear function of the signal input to it, meaning that a network built from interacting thermodynamic neurons can function as a universal approximator [20, 21]. Within a digital simulation of a thermodynamic computer we construct networks of such neurons using the bilinear interactions characteristic of existing thermodynamic computers [11, 12]. We train these computers by genetic algorithm to perform nonlinear computations – expressing a nonlinear function and classifying MNIST – at specified times. Thermodynamic computers

\* [swhitelam@lbl.gov](mailto:swhitelam@lbl.gov)

† [ccasert@lbl.gov](mailto:ccasert@lbl.gov)

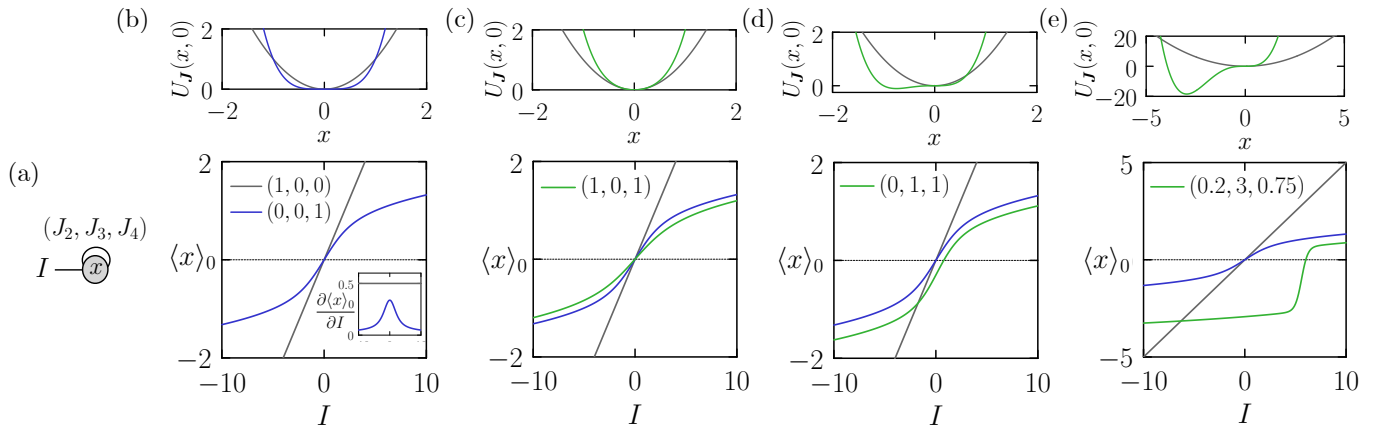


FIG. 1. (a) A thermodynamic circuit whose interaction energy is given by Eq. (1) can function as a thermodynamic neuron. In panels (b–e) we show the equilibrium activation function  $\langle x \rangle_0$  of the neuron, Eq. (2), as a function of the neuron input  $I$ , for the case  $\beta = 1$ . The vector  $\mathbf{J} = (J_2, J_3, J_4)$  sets the values of the intrinsic couplings of the neuron. The top panels in (b–e) show the potential (1) at zero input, for the quadratic case (gray) and the case introduced in the lower panel (blue or green). (b) Purely quadratic (gray) and quartic (blue) cases. The purely quartic case (with  $J_4 > 0$ ) is the simplest case that is thermodynamically stable and admits a nonlinear activation function. Both cases are shown for reference in the following panels. Inset: gradient of activation function on the same horizontal scale as the main panel. (c) Example in which a quadratic coupling is included with the quartic coupling. (d) Example in which a cubic coupling is included with the quartic coupling. (e) Example in which all three couplings are nonzero.

of this nature could be considered to be thermodynamic neural networks, or “thermoneural networks”.

This results of this paper expand the field of thermodynamic computing beyond linear algebra and thermodynamic equilibrium, enabling fully nonlinear computations, comparable to those performed by conventional neural networks, at specified observation times. The design and training of the computer are done by ‘digital twin’, applying a genetic algorithm to a simulation model of the thermodynamic computer realized on a classical digital computer. The elements of the present design have been implemented in hardware [11, 12], with the exception of the quartic neuron potential. If the latter can be engineered – perhaps by using nonlinear inductors or capacitors to induce quartic self-interactions within RLC circuits, or using the nonlinear inductance provided by Josephson junctions [22] – then the resulting nonlinear computer can be programmed, e.g. by genetic algorithm. The result would be a thermodynamic computer that would be driven by thermal fluctuations to perform a specified computation at a specified observation time, whether or not the computer has come to equilibrium.

This work adds to the literature of classical models that can be used to perform calculations, such as Hopfield networks [23], Boltzmann Machines [24], physical neural networks [25], and charge-based thermodynamic neural networks that self-organize under external drive [6]. Our design is analogous to conventional perceptron-based neural networks in that it is programmable and can function as a universal approximator, but differs in that it is stochastic and designed to be implemented in hardware, where its operation would be driven by the natu-

ral dynamics of fluctuating classical degrees of freedom. A recent paper [26] presented the design for a thermodynamic neuron realized by qubits coupled to multiple thermal baths. The design presented here is based on a fully classical model of a nonlinear thermodynamic neuron, and requires only a single thermal bath.

In Section II we introduce and analyze the properties of a simple thermodynamic circuit that can function as a thermodynamic neuron, a fluctuating degree of freedom whose output is a nonlinear function of its input. In Section III we simulate interacting networks of thermodynamic neurons, and train them by genetic algorithm to perform specified nonlinear computations. We conclude in Section IV.

## II. THERMODYNAMIC NEURONS

### A. Equilibrium behavior

To motivate the construction of a thermodynamic computer analogous to a neural network, consider the thermodynamic circuit shown in Fig. 1(a). This circuit represents a scalar degree of freedom  $x$  that experiences the potential energy

$$U_{\mathbf{J}}(x, I) = J_2 x^2 + J_3 x^3 + J_4 x^4 - Ix. \quad (1)$$

The parameters  $\mathbf{J} = (J_2, J_3, J_4)$  are the intrinsic couplings of the circuit, and  $I$  is an input signal. We can consider the circuit to represent a thermodynamic neuron, whose activation function is the relation between the

output  $x$  and the input  $I$ . The output must be a non-linear function of the input in order for a network built from such neurons to be a universal approximator.

Let the neuron be put in contact with a thermal bath at temperature  $T$ . Our ultimate goal is to consider networks of such neurons operating at specified observation times, but an important design consideration in pursuit of this goal is the equilibrium behavior of a single neuron. In thermal equilibrium, the output of the neuron has the mean value

$$m = \langle x \rangle_0, \quad (2)$$

where

$$\langle \cdot \rangle_0 \equiv \frac{\int dx (\cdot) e^{-\beta U_{\mathbf{J}}(x, I)}}{\int dx e^{-\beta U_{\mathbf{J}}(x, I)}}. \quad (3)$$

When the neuron potential is purely quadratic, i.e.  $\mathbf{J} = (J_2, 0, 0)$  – with  $J_2 > 0$  to ensure thermodynamic stability – the integrals in (3) can be solved analytically, giving the linear form  $m = I/(2J_2)$ . This form is plotted, for  $J_2 = 1$ , as a gray line in Fig. 1(b); the horizontal dotted black line denotes the value zero. In this case the equilibrium activation function of the neuron is linear, meaning that networks of such neurons in equilibrium cannot serve as universal function approximators [27].

The simplest case that is thermodynamically stable and admits a nonlinear equilibrium activation function is the purely quartic case,  $\mathbf{J} = (0, 0, J_4)$ , with  $J_4 > 0$ . This case is shown as a blue line in Fig. 1(b), with  $J_4 = 1$  [28]. The equilibrium activation function is nonlinear: its gradient (shown inset) is largest near the origin, and decreases as  $|I|$  becomes large. The gradient remains finite for finite  $I$ : the neuron does not saturate.

Panels (c), (d), and (e) of Fig. 1 show the effect on the thermodynamic neuron's equilibrium activation function of including quadratic and cubic terms with the quartic coupling. The resulting activation functions display a range of forms that resemble some of those used in classical neural networks, notably the sigmoid and hyperbolic tangent functions [29–31].

The quartic coupling alone renders the activation function of the thermodynamic neuron nonlinear in equilibrium. However, an additional design consideration is the variance  $\sigma^2$  of the neuron's equilibrium fluctuations, where

$$\sigma^2 = \langle x^2 \rangle_0 - \langle x \rangle_0^2. \quad (4)$$

In Fig. 2(a) we plot the value of (4) as a function of neuron input  $I$  for the quadratic case  $\mathbf{J} = (1, 0, 0)$  (gray) and the quartic case  $\mathbf{J} = (0, 0, 1)$  (blue). In the quadratic case the variance is constant for constant temperature,  $\sigma^2 = 1/(2\beta)$ , reflecting the equipartition theorem. In the quartic case the variance is not constant, and is largest near  $I = 0$ ; the inset shows that its maximum value is several times that of the quadratic neuron. The mixed quadratic-quartic case  $\mathbf{J} = (1, 0, 1)$ , shown green

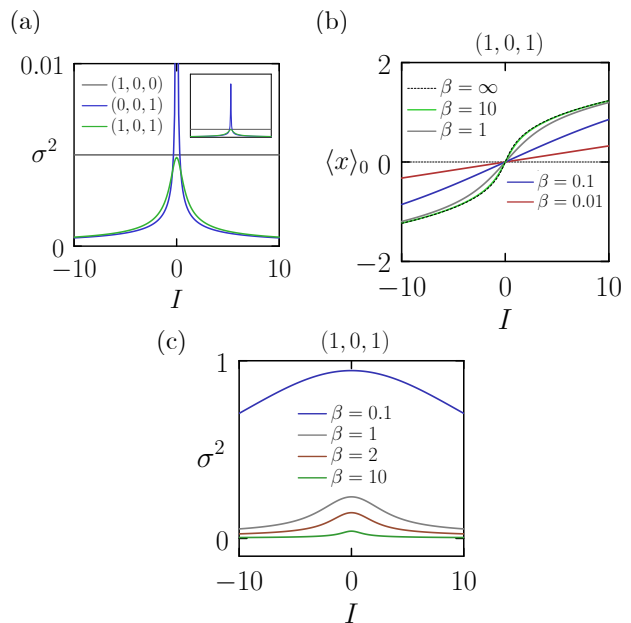


FIG. 2. (a) Equilibrium fluctuations (4) of the thermodynamic neuron of Fig. 1(a), for the case  $\beta = 100$ . The addition of the quadratic coupling to the quartic one (green), suppresses fluctuations relative to the pure quartic case (blue). The *mean* equilibrium activation functions of those two cases are similar; see Fig. 1(c). The inset shows the largest fluctuations of the purely quartic neuron to be many times that of the purely quadratic neuron. (b,c) The mean (b) and variance (c) of the equilibrium activation function of the  $(1, 0, 1)$  neuron depend on temperature.

in Fig. 1(c), has fluctuations at the origin comparable to the quadratic case, while the *mean* activation function of the case  $(1, 0, 1)$ , shown in Fig. 1(c), is similar to that of the pure quartic case. The addition of the quadratic term to the quartic one suppresses fluctuations without changing the essence of the nonlinearity.

The larger the fluctuations of a thermodynamic neuron's output, the more samples will be required to compute a meaningful signal when observing a computer built from such neurons. For these reasons we choose our default neuron parameters to be  $\mathbf{J} = (1, 0, 1)$ : the quartic coupling induces nonlinearity, while the quadratic coupling serves to suppress fluctuations near  $I = 0$ .

The equilibrium activation function of a nonlinear thermodynamic neuron depends on temperature. In Fig. 2(b) and (c) we show the mean and variance of the equilibrium activation function of the neuron  $\mathbf{J} = (1, 0, 1)$  for a range of values of  $\beta$ . The mean activation is nonlinear provided that temperature is not much larger than the scales of  $J_2$  and  $J_4$ . The case in which they are comparable, i.e.  $|J_2|/k_B T \approx J_4/k_B T \approx 1$ , is acceptably nonlinear. Under the same conditions, the variance  $\sigma^2$  of the equilibrium activation function, panel (b), is generally comparable in scale to the mean of the function.

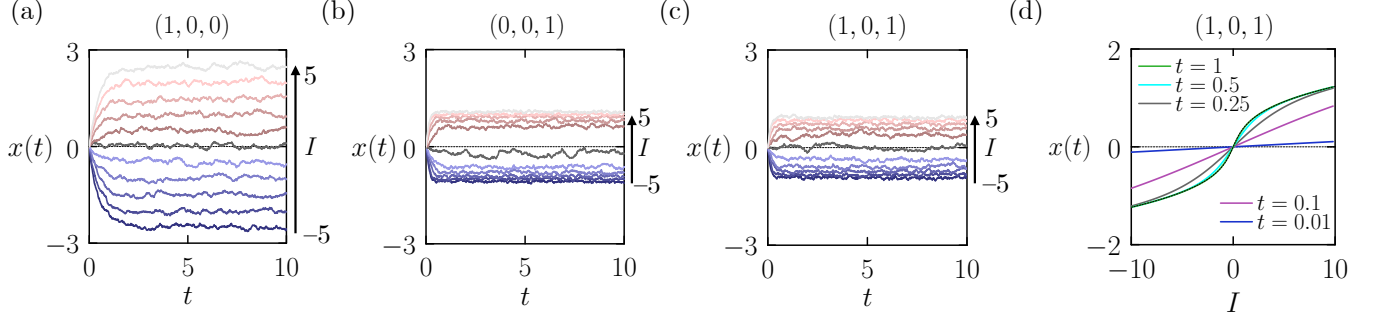


FIG. 3. Nonequilibrium properties of the thermodynamic neuron of Fig. 1(a). (a–c) Langevin evolution (5) of the neuron  $x$  for  $\beta = 100$ , for 11 evenly-spaced values of  $I$ . We consider three different sets of couplings  $\mathbf{J}$ : (a) purely quadratic; (b) purely quartic; and (c) mixed quadratic-quartic. (d) The finite-time activation function of the (1,0,1) neuron under the dynamics (5) (here for  $\beta = \infty$ ) is nonlinear above some threshold observation time (here about 0.2 time units), and for longer times converges to the equilibrium result (curved black dashed line).

### B. Nonequilibrium behavior

Having assessed the equilibrium behavior of the thermodynamic neuron of Fig. 1(a), we turn to its dynamical behavior. Thermodynamic computers operate under Langevin dynamics, both overdamped and underdamped [11, 12]. In this paper we will simulate the behavior of a thermodynamic computer using overdamped Langevin dynamics, in which case our single thermodynamic neuron evolves according to the equation [32]

$$\dot{x} = -\mu \frac{\partial}{\partial x} U_{\mathbf{J}}(x, I) + \sqrt{2\mu k_B T} \eta(t), \quad (5)$$

where  $U_{\mathbf{J}}(x, I)$  is given by Eq. (1). Here  $\mu$ , the mobility parameter, sets the basic time constant of the computer. For the thermodynamic computers of Refs. [11, 12],  $\mu^{-1} \sim 1$  microsecond. For damped oscillators made from mechanical elements [33] or Josephson junctions [22], the time constant would be of order a millisecond or a nanosecond, respectively. The second term on the right-hand side of Eq. (5) represents the thermal fluctuations of the heat bath;  $\eta$  is a Gaussian white noise satisfying  $\langle \eta(t) \rangle = 0$  and  $\langle \eta(t)\eta(t') \rangle = \delta(t - t')$ .

In Fig. 3(a)–(c) we show the dynamical evolution of the neuron  $x$  under the dynamics (5), starting from  $x = 0$ , for various fixed values of the input  $I$ . Here  $\beta = 100$ . Panel (a) shows the evolution of (5) for the case of a purely quadratic coupling,  $\mathbf{J} = (1, 0, 0)$ . Time traces for 11 values of  $I$  are shown, evenly spaced from  $-5$  to  $5$ . The neuron is initially out of equilibrium, converging to equilibrium in about 2 time units (time is expressed in units of  $\mu^{-1}$ ). As described by Fig. 1(b), the mean value of  $x$  in equilibrium is a linear function of  $I$ . As described by Fig. 2(a), the size of the neuron's fluctuations in equilibrium is independent of  $I$ .

Fig. 3(b) shows the case of a purely quartic coupling,  $\mathbf{J} = (0, 0, 1)$ . Again, time traces for 11 values of  $I$  are shown, evenly spaced from  $-5$  to  $5$ ; these converge at sufficiently long times to a nonlinear function  $x(I)$ . As

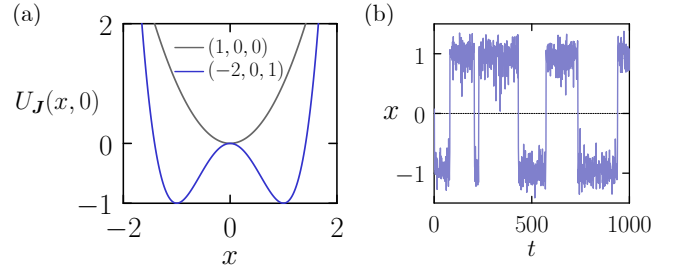


FIG. 4. (a) Bistable neuron potential (blue) at zero input, and (b) the resulting neuron dynamics (5) for  $\beta = 5$ .

described by Fig. 2(a), the fluctuations of  $x$  are largest for  $I = 0$ .

Fig. 3(c) shows the case of a mixed quadratic-quartic coupling,  $\mathbf{J} = (1, 0, 1)$ . The long-time mean activation function is nonlinear in  $I$ , and, as described by Fig. 2(a), the fluctuations near  $I = 0$  are suppressed relative to the purely quartic case of panel Fig. 3(b).

From these plots we see that for short times (here less than about 2 time units) the thermodynamic neuron's finite-time activation function does not equal the equilibrium (long-time) activation function. In Fig. 3(d) we show the value of  $x$ , derived from Eq. (5), for a range of values of the input  $I$ , for various fixed values of  $t$  (here we set  $\beta = \infty$ ). For times shorter than about 0.2 units, the finite-time activation function of the neuron is linear on the scale of the inputs shown. Thus a network of such neurons would not function as a universal approximator if observed on such timescales. For longer times, however, the finite-time activation function of the neuron is nonlinear on the scale of the inputs shown. As long as we observe the output of a thermodynamic neural network on timescales longer than this threshold, it will behave as a nonlinear model. As observation time increases, the finite-time activation function of the thermodynamic neuron converges to the long-time equilibrium activation function of the neuron, which we have designed to be

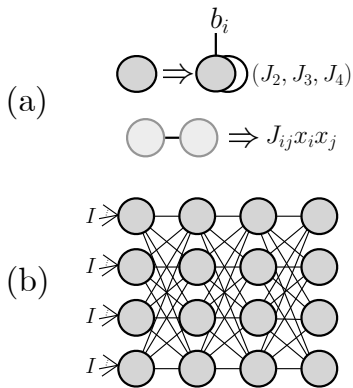


FIG. 5. Elements of a thermodynamic computer analogous to a neural network. (a) The thermodynamic neurons described in Figs. 1–3 are connected by bilinear couplings. (b) We consider layered networks of such neurons (adjacent layers are coupled all-to-all), with total potential energy (8).

nonlinear.

For certain values of the intrinsic couplings  $\mathbf{J}$ , a thermodynamic neuron can display multistability. For example, the potential (1) with  $\mathbf{J} = (-|J_2|, 0, J_4)$  displays two minima at activations  $x_0 = \pm\sqrt{J_2^2/(2J_4)}$ , separated by a potential energy barrier of size  $J_2^2/(4J_4)$ . One example of such a potential is shown in Fig. 4(a), compared with the quadratic potential (gray). The resulting dynamics (5) at zero input shows intermittency, as shown in Fig. 4(b). Bistable neurons possess nonlinear activation functions in the vicinity of their stable states, but can also exhibit abrupt changes between states. Such bistability could be used for robust memory storage, or as a mechanism for noise-robust classification in thermodynamic neural networks. In the remainder of this paper we consider only monostable neurons. To summarize the design considerations of this section: 1) the thermodynamic neuron of Fig. 1(a) has a nonlinear equilibrium activation function if it possesses a quartic nonlinearity; 2) it is useful to also include a quadratic nonlinearity in order to suppress equilibrium fluctuations near zero neuron input; and 3) for observation times longer than some threshold, such a neuron also possesses a finite-time activation function that is nonlinear. As a result, networks of such neurons can serve as universal function approximators, both in and out of equilibrium. In the following section we illustrate these properties.

### III. PROGRAMMING A THERMODYNAMIC COMPUTER

#### A. A digital model of a thermodynamic universal approximator

Networks of nonlinear neurons are universal approximators [20, 21]. Networks of nonlinear thermodynamic

neurons are universal approximators whose operation is driven by thermal fluctuations. In this section we show that such networks can be designed on a digital computer and programmed to perform specified computations at specified observation times.

Consider a graph of  $N$  thermodynamic neurons  $x_i$ , with potential energy function

$$V_{\text{int}}(\mathbf{x}) = \sum_{i=1}^N U_{\mathbf{J}}(x_i, b_i) + \sum_{\text{conn}(ij)} J_{ij} x_i x_j. \quad (6)$$

The subscript ‘int’ stands for ‘internal’, and ‘conn’ for ‘connections’. The first sum in (6) runs over  $N$  single-neuron energy terms (1), with the intrinsic couplings of each neuron set by the vector  $\mathbf{J} = (J_2, J_3, J_4)$ . Our default choice is  $(1, 0, 1)$ . We will also consider the linear-model case  $(1, 0, 0)$ , in order to demonstrate the difference in expressive power between a linear model and a nonlinear one. The input  $b_i$  to each neuron serves as a bias.

The second sum in (6) runs over all distinct pairs of connected neurons, which are determined by the graph structure imposed. We use the bilinear interaction of Refs. [11, 12]. The computers described in those papers use an all-to-all coupling; here, to make contact with existing neural-network designs, we consider the layered structure shown in Fig. 5, with all-to-all connections between layers. This design mimics that of a conventional deep fully-connected neural network. However, unlike in a conventional deep neural network, in which information flows from the input layer to the output layer, the bilinear interaction  $J_{ij}x_i x_j$  ensures that neuron  $i$  communicates with neuron  $j$ , and vice versa, and so information flows forward *and* backward between the layers of the thermodynamic computer.

To provide input to the thermodynamic computer we introduce the external coupling

$$V_{\text{ext}}(\mathbf{x}, \mathbf{I}) = \sum_{\text{inputs}(ij)} W_{ij} I_i x_j, \quad (7)$$

where the sum runs over all connections between the external inputs  $I_i$  and the input neurons  $x_j$  (here the top-layer neurons), mediated by the parameters  $W_{ij}$ . The total potential energy of the thermodynamic computer is then

$$V(\mathbf{x}) = V_{\text{int}}(\mathbf{x}) + V_{\text{ext}}(\mathbf{x}, \mathbf{I}). \quad (8)$$

We assume the computer to be in contact with a thermal bath, and to evolve in time according to the overdamped Langevin dynamics

$$\dot{x}_i = -\mu \frac{\partial V(\mathbf{x})}{\partial x_i} + \sqrt{2\mu k_B T} \eta_i(t), \quad (9)$$

where  $V(\mathbf{x})$  is given by Eq. (8). The Gaussian white noise terms satisfy  $\langle \eta_i(t) \rangle = 0$  and  $\langle \eta_i(t) \eta_j(t') \rangle = \delta_{ij} \delta(t - t')$ .



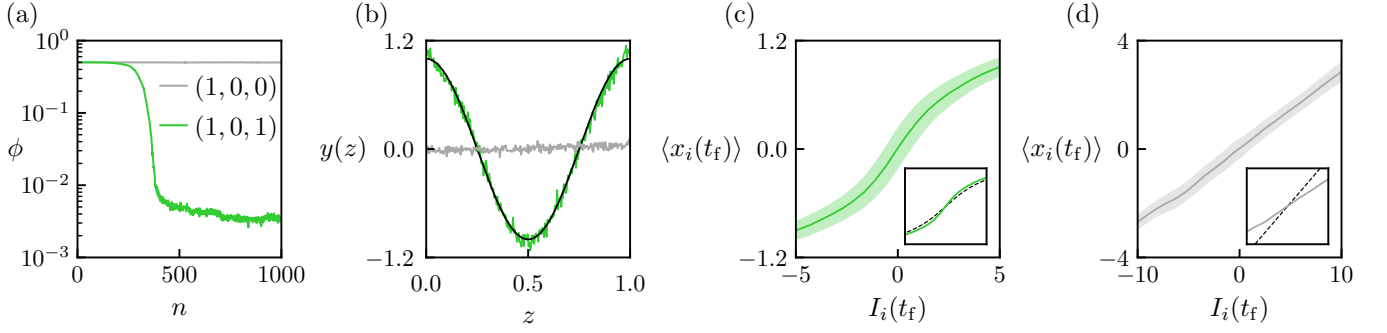


FIG. 6. Training a simulation model of a thermodynamic computer to express a nonlinear function at a specified observation time. (a) Loss (14) as a function of evolutionary time  $n$  for a layered thermodynamic computer (see Fig. 5) with quadratic neurons (gray) or quadratic-quartic neurons (green). (b) Output (15) at observation time  $t_f = 1$  of the linear computer (gray) and the nonlinear computer (green), as a function of the input  $z$ , averaged over  $M = 10^3$  samples. The target function (13) is shown as a black line. (c,d). Mean neuron activations measured at observation time  $t_f$  as a function of the neuron inputs at the same time, for (c) the nonlinear model and (d) the linear model. The color bands denote  $\pm$  one standard deviation. Insets: the measured activation at  $t_f$  compared with the *equilibrium* neuron activation (2).

We designate the final-layer neurons to be the output neurons. We will consider loss functions  $\phi$  that are function of the outputs

$$\{x_i(\mathbf{I}, t)\}, i \in \text{outputs}. \quad (10)$$

Here  $\mathbf{I}$  is the vector of inputs, and  $x_i(\mathbf{I}, t)$  denotes the outcome of the dynamics (9) for neuron  $i$  at time  $t$  upon starting from zero neuron activations,  $\mathbf{x} = \mathbf{0}$  (all dynamical trajectories start from zero neuron activations).

Because the computer is noisy, we wish to take  $M$  samples of each output and average over these samples. We will consider two types of sampling. The first is reset sampling. In this mode of operation we run the computer for time  $t_f$ , observe the outcome, reset the neuron activations to zero, and repeat the procedure  $M - 1$  times, gathering  $M$  samples in total. The advantage of this mode of sampling is that it naturally lends itself to parallelization: the  $M$  samples can be computed independently, on distinct copies of the thermodynamic computer if such copies are available. Reset sampling can also be done using a single computer whose neurons are reset periodically. The reset-sampling average is

$$\langle x_i(\mathbf{I}) \rangle_r = M^{-1} \sum_{\alpha=1}^M x_i^{(\alpha)}(\mathbf{I}, t_f), \quad (11)$$

where the sum runs over  $M$  independent realizations  $\alpha$  of the dynamics (9). The only requirement on  $t_f$  is that it is long enough that the effective activation function of the neuron is nonlinear. From the considerations of Section II B, we set  $t_f = 1$  (in units of  $\mu^{-1}$ ).

We also consider serial sampling, taking  $M$  samples at intervals  $t_{\text{obs}}$  from a single computer running continuously for time  $t_f = Mt_{\text{obs}}$ . In this case the relevant average is

$$\langle x_i(\mathbf{I}) \rangle_s = M^{-1} \sum_{\alpha=1}^M x_i(\mathbf{I}, \alpha t_{\text{obs}}), \quad (12)$$

where the sum runs over  $M$  samples within a single trajectory. Serial sampling is used in equilibrium in Refs. [11, 12]. In equilibrium, a burn-in time is required for the computer to attain equilibrium, and the observation time must be long enough to obtain uncorrelated equilibrium samples. Here, by contrast, we do not require that any portion of the trajectory correspond to equilibrium (it may do, but it is not required to). As a result, we require only that  $t_{\text{obs}}$  be long enough for the model to be nonlinear (from the considerations of Section II B, we set  $t_{\text{obs}} = 0.2$ , in units of  $\mu^{-1}$ ). No burn-in time is required, and samples do not need to be uncorrelated.

## B. Programming the computer

In what follows we consider the adjustable parameters of the computer to be the set  $\theta = \{W_{ij}\} \cup \{b_i\} \cup \{J_{ij}\} \cup \{f_i\}$ . Here  $\{W_{ij}\}$  is the set of input weights specified by Eq. (7);  $\{b_i\}$  is the set of biases specified by Eq. (6);  $\{J_{ij}\}$  is the set of connections specified by the same equation; and  $\{f_i\}$  is a set of weights that couple to the output neurons (see Section III C).

To program the computer we adjust the parameters  $\theta$  using a genetic algorithm instructed to minimize a loss function  $\phi$ . The loss is constructed from the  $M$  samples (11) or (12) for all output neurons, and is evaluated for  $K$  different sets of inputs. This evaluation requires  $KM$  dynamical trajectories in reset-sampling mode, and  $K$  dynamical trajectories in serial-sampling mode (loss functions are specified in Section III C and Section III D). We consider a population of  $P = 50$  thermodynamic computers, each of which is initialized with random parameters  $\theta_i \sim \mathcal{N}(0, 10^{-2})$ . We evaluate  $\phi$  for each computer, and select the 5 computers associated with the smallest values of  $\phi$ . These 5 are cloned and mutated to produce a new population of 50 computers. Mutations are done by adding to each parameter of each computer a Gaus-

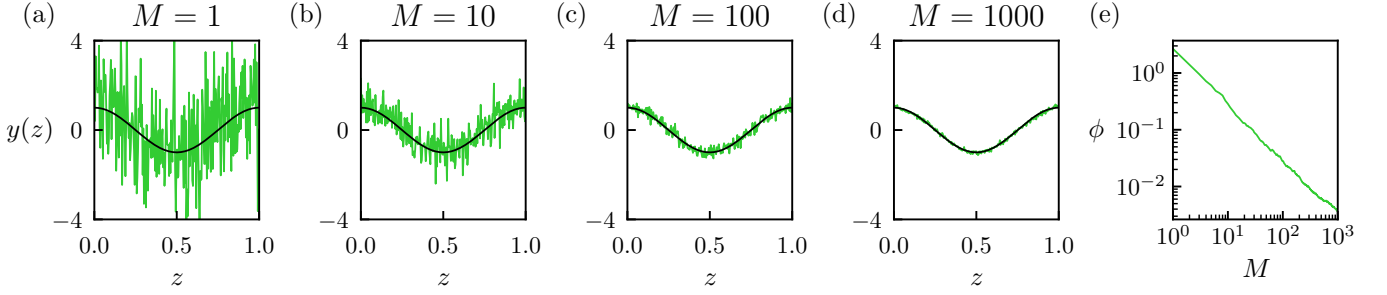


FIG. 7. (a-d) Output (15) at time  $t_f = 1$  of the trained nonlinear thermodynamic computer as a function of input  $z$ , computed using  $M$  samples. The target function (13) is shown as a black line (training was done using  $M = 10^3$  samples). (e) Loss (14) as a function of  $M$ .

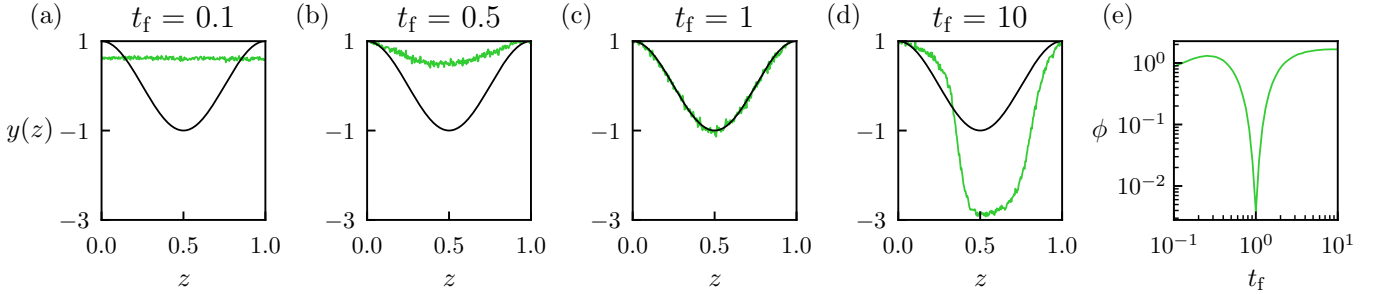


FIG. 8. (a-d) Output (15) at various observation times  $t_f$  of the trained nonlinear thermodynamic computer, as a function of input  $z$ , computed using  $M = 10^3$  samples. The target function (13) is shown as a black line. The computer is trained so that it reproduces the target function when observed at time  $t_f = 1$ . (e) Loss (14) as a function of observation time  $t_f$ .

sian random number  $\epsilon \sim C^{-1/2}\mathcal{N}(0, 10^{-2})$ . The term  $C$  is the *fan-in*. It is equal to 1 for biases  $b_i$  or weights  $f_i$ ; it is equal to  $N_j$  for weights  $W_{ij}$ , where  $N_j$  is the number of connections entering neuron  $j$ ; and it is equal to  $(N_i + N_j)/2$  for weights  $J_{ij}$ . Scaling mutations by the fan-in ensures that changes to all neuron inputs are of similar scale even if the network is strongly heterogeneous [34] (similar scaling ideas were used when developing efficient implementations of gradient descent [35]). Values of  $\phi$  for the new population are calculated, the best 5 are selected, and so on.

We developed an efficient implementation of a genetic algorithm for GPU. In reset-sampling mode, each step of the genetic algorithm requires the evaluation of  $PKM$  dynamical trajectories of length  $t_f$  ( $KM$  trajectories per computer to construct the loss function  $\phi$ , with  $P$  computers in the genetic population). In serial-sampling mode, each step of the genetic algorithm requires the evaluation of the  $PK$  dynamical trajectories of length  $t_f = Mt_{\text{obs}}$ . All trajectories can be evaluated in parallel on a set of GPUs.

Following training, the identity of the computer's parameters are fixed, and the computer can be run for any chosen input. In reset-sampling mode, testing or inference can be done with fewer than  $M$  samples, if desired, as we shall describe. The parameters of the digital model of the thermodynamic computer could in principle be implemented in hardware, with the result being a device

designed to output a specified computation at a specified time (or set of times, in the case of serial sampling), powered by thermal fluctuations. We note that if the hardware implementation is not an exact copy of the digital model, genetic-algorithm training could be continued directly in hardware: the procedure can be applied to an experimental system exactly as it is applied to a simulation model [36].

### C. Learning a nonlinear function

To demonstrate the training and operation of a thermodynamic computer analogous to a neural network, we consider the task of expressing a nonlinear function of a single variable. In this case the computer has one input. We define the target function

$$y_0(z) \equiv \cos(2\pi z), \quad (13)$$

and the loss function

$$\phi \equiv K^{-1} \sum_{j=1}^K (y_0(z_j) - y(z_j))^2. \quad (14)$$

Here the sum runs over  $K = 250$  evenly-spaced points  $z_j = j/(K-1)$  on the interval  $z \in [0, 1]$ . The quantity

$$y(z) \equiv \sum_{i \in \text{outputs}} f_i \langle x_i(z) \rangle_{\text{r,s}} \quad (15)$$

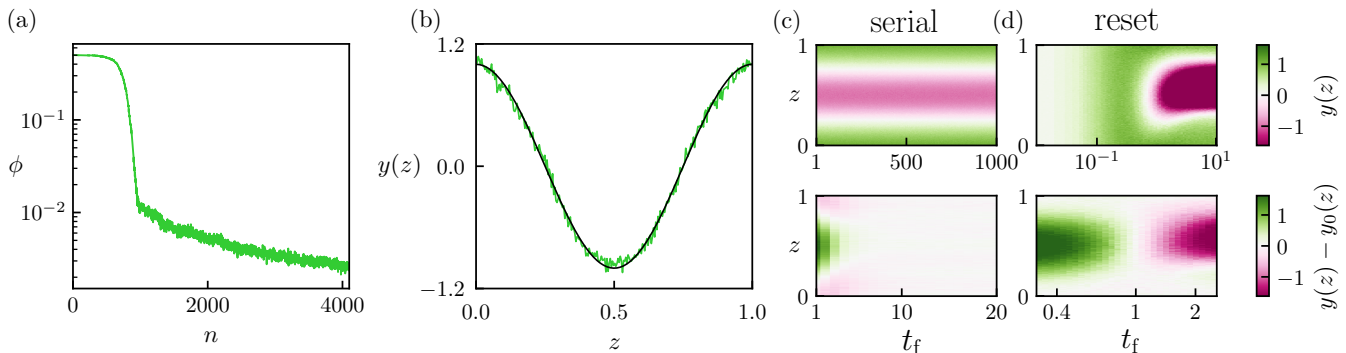


FIG. 9. Training a simulation model of a thermodynamic computer to express a nonlinear function in serial-sampling mode. (a) Loss (14) as a function of evolutionary time  $n$  for a layered thermodynamic computer (see Fig. 5) with quadratic-quartic (1,0,1) neurons. (b) Output (15) of the thermodynamic computer, evaluated using  $M = 10^3$  time slices, evenly spaced from  $t_{\text{obs}} = 0.2$  to time  $t_f = Mt_{\text{obs}} = 200$  (see Eq. (12)). The black line is the target function  $y_0(z)$ , Eq. (13). (c) Color maps of the output  $y(z)$  of the trained computer, evaluated using  $M = 10^3$  evenly-spaced time slices up to time  $t_f$ . The bottom panel shows the difference between the computer output and the target function. The steady-state output of the computer remains close to the target function for a range of observation times. (d) Analogous plots for the computer trained in reset-sampling mode (see Figs. 6–8); here, the computer approximates the target function only at the observation time specified in training ( $t_f = 1$ ).

is the output of the thermodynamic computer, given the input  $z$ , averaged over  $M$  samples (either in reset-sampling mode (11) or serial-sampling mode (12)). To integrate Eq. (9) we use a first-order Euler scheme with timestep  $\Delta t = 10^{-3}$ . We take  $M = 10^3$  for the purposes of training. The  $f_i$  are parameters trained by the genetic algorithm.

We choose a layered computer design of width 8 and depth 4. We consider two types of thermodynamic neuron: a quadratic-quartic thermodynamic neuron,  $\mathbf{J} = (1, 0, 1)$ , which gives rise to a nonlinear computer, and a quadratic thermodynamic neuron,  $\mathbf{J} = (1, 0, 0)$ , which gives rise to a linear computer. We take  $\beta = 10$ , so that the neuron energy scale is 10 times that of the thermal energy, i.e.  $J_{2,4}/k_B T = 10$ .

In Fig. 6(a) we show the loss as a function of evolutionary time for the two models, in reset-sampling mode. The linear model fails to train – it cannot express a nonlinear function of the input variable – while the nonlinear model learns steadily, reaching a small value of the loss. Panel (b) shows the output functions learned by the two models: the nonlinear model has learned a good approximation of the target cosine function. The intrinsic noise of the computer is visible in the output, but for  $M = 10^3$  samples, for each value of  $z$ , the mean output signal of the computer exceeds the scale of the noise by a considerable margin.

Panels (c) and (d) of Fig. 6 show the sampled neuron outputs as a function of the neuron inputs (the inputs being all signals in to the neuron, excepting the thermal noise) at the designated observation time,  $t_f = 1$ . Consistent with the considerations of Section II, the nonlinear model possesses a nonlinear finite-time activation function, indicating that we are beyond the nonlinear threshold observation time. The resulting nonlinear ac-

tivation function explains the computer’s ability to learn an arbitrary nonlinear function. Panel (d) confirms that the quadratic-neuron computer is at finite times a linear model, as expected.

In the inset to the two panels we show the equilibrium activation functions of the two neurons. These are qualitatively similar to their finite-time counterparts – nonlinear or linear, respectively – but different in detail. For the nonlinear model this difference is unimportant. Our aim is to express the target function at a finite observation time, and so what matters is that the finite-time observation time is nonlinear (which is the case if observed on timescales longer than the nonlinear threshold time). The fact that the equilibrium activation function is nonlinear simply ensures that the finite-time activation function will remain nonlinear, however long our observation time.

Training is done using  $M = 10^3$  samples for each value of the input  $z$ , but the trained computer can be used with fewer than  $M$  samples if desired. In Fig. 7 we show the output of the trained thermodynamic computer, as a function of the input  $z$ , for a range of values of  $M$ . The number of samples can be chosen in order to achieve a required precision.

Training in reset-sampling mode results in a thermodynamic computer programmed to express the target function at a prescribed observation time  $t_f = 1$ . In Fig. 8 we show the output of the computer at a range of observation times. The output of the computer varies as a function of time, and is equal to the target function only at the prescribed observation time. The output of the computer in equilibrium (corresponding to the long-time limit) is considerably different to the target function. In this example, therefore, the programmed thermodynamic computer operates far from equilibrium.



The model thermodynamic computer can also be trained in serial-sampling mode, as shown in Fig. 9. In this case the thermodynamic computer produces a trajectory whose stationary state approximates the target function over a range of observation times. The requirement of training is that, given an input  $z$ , the output of the computer, averaged over  $M = 10^3$  samples taken at evenly-spaced times, from  $t_{\text{obs}} = 0.2$  to time  $t_f = Mt_{\text{obs}} = 200$ , be as close as possible to the target function,  $y_0(z)$ , Eq. (13). In the top image of panel (c) we show the output of the *trained* computer, averaged over  $M = 10^3$  time slices, up to various  $t_f$ . The output of the trained computer remains close to the target function for a wide range of observation times. The lower image in panel (c) shows the difference between the computer output and the target function: after an initial transient (which is included in the serial-sampling average (12)), the computer achieves a steady-state output that approximates the target function. This steady state may correspond to a true thermodynamic equilibrium, but we did not require this: the training requirement was only that the computer achieve a given output when averaged over a specific time interval.

The color maps in Fig. 9(d) show similar quantities for the computer trained in reset-sampling mode (see Figs. 6–8). In this mode the computer was trained to approximate the target function using  $M = 10^3$  samples taken at a single observation time,  $t_f = 1$  (see Eq. (11)). As shown by the color plots (derived from  $10^3$  samples from the trained computer taken at observation time  $t_f$ ), the output of the computer approximates the target function only at time  $t_f = 1$ .

#### D. Classifying MNIST

Having confirmed the ability of a network of nonlinear thermodynamic neurons to express an arbitrary nonlinear function, we now consider a standard benchmark in machine learning, classifying the MNIST data set [37]. MNIST consists of greyscale images of 70,000 handwritten digits on a grid of  $28 \times 28$  pixels, each digit belonging to one of ten classes  $C \in [0, 9]$ .

As in Section III C, we take  $\beta \equiv (k_B T)^{-1} = 10$ , so that the neuron energy scale is 10 times that of the thermal energy, i.e.  $J_{2,4}/k_B T = 10$ . We consider a 3-layer thermodynamic computer with quadratic-quartic (1, 0, 1) neurons. Each layer has 32 neurons. Each neuron in the input layer couples to all the pixels  $I_i$  of an MNIST digit via Eq. (7). The output layer of 32 neurons is used to construct the computer's prediction for the class of MNIST digit  $I_j$ , via the 10 expressions

$$y^{(C)}(\mathbf{I}) \equiv \sum_{i \in \text{outputs}} f_i^{(C)} \langle x_i(\mathbf{I}) \rangle_r. \quad (16)$$

Here  $C \in [0, 9]$  is the class index, and the  $f_i^{(C)}$  are 320 parameters that will be trained by genetic algorithm. Recall that the reset-sampling average is specified by Eq. (11).

We train the computer in reset-sampling mode, with  $M = 10^3$  samples taken at observation time  $t_f = 1$ . For the loss function we choose the cross-entropy between the class probabilities predicted by the thermodynamic computer and the ground-truth labels. The probability  $p^{(C)}$  that a given digit  $\mathbf{I}_j$  is of class  $C$  is obtained by applying a softmax transformation to (16),

$$p^{(C)}(\mathbf{I}_j) = \frac{\exp[y^{(C)}(\mathbf{I}_j)]}{\sum_{C'=0}^9 \exp[y^{(C')}(\mathbf{I}_j)]}, \quad (17)$$

and the cross-entropy, our loss function, is

$$\phi = -\frac{1}{K} \sum_{j=1}^K \sum_{C=0}^9 \hat{p}_k^{(C)}(\mathbf{I}_j) \ln p_k^{(C)}(\mathbf{I}_j). \quad (18)$$

Here  $\hat{p}$  is the ground-truth label, unity if  $\mathbf{I}_j$  is of class  $C$  and zero otherwise. The sum is taken over all  $K = 60,000$  training samples, i.e. we use full-batch learning.

This cross-entropy is used only in training: the expressions (17) and (18) are not intended to be implemented in hardware. Once trained, the computer can be used to do classification, which we do intend to be implementable using analog hardware. Classification is done by measuring which of the 10 quantities (16) is largest, when the computer is connected to a given digit. If the thermodynamic computer is realized in hardware, each of the outputs (16) could be connected to a tree of comparators and a multiplexer. This additional hardware could be used to determine the identity of the quantity with the largest value, and hence the computer's predicted class for the digit.

Each evolutionary generation consists of 48 simulated thermodynamic computers, each shown 60,000 digits. Each digit is shown to each computer 1000 times, and the computer is allowed to run for time  $t_f$  each time. We therefore simulate  $2.9 \times 10^9$  trajectories of length  $t_f$  per generation, which we parallelize over 96 GPUs. Training was done for over 4000 generations (of order 24 hours of run time), and so required the generation of more than  $10^{13}$  trajectories. Training this thermodynamic computer is therefore much more expensive than training a conventional deep neural network, which can be trained to classify MNIST in seconds on a conventional computer. The advantage of the thermodynamic approach is that, once trained, the parameters can be implemented in hardware, where the computer program will run automatically, driven only by thermal fluctuations. Conventional neural networks, once trained, must still be evaluated by explicit input of power to a CPU or GPU. Nonetheless, it will be beneficial to find less costly methods for training thermodynamic computers.

In Fig. 10(a) we show the loss (18) as a function of evolutionary time  $n$  as the computer is trained to classify MNIST. The computer learns steadily under the action of the genetic algorithm. Panel (b) shows the corresponding training-set classification accuracy (which can be observed but is not used during training). Panel (c)

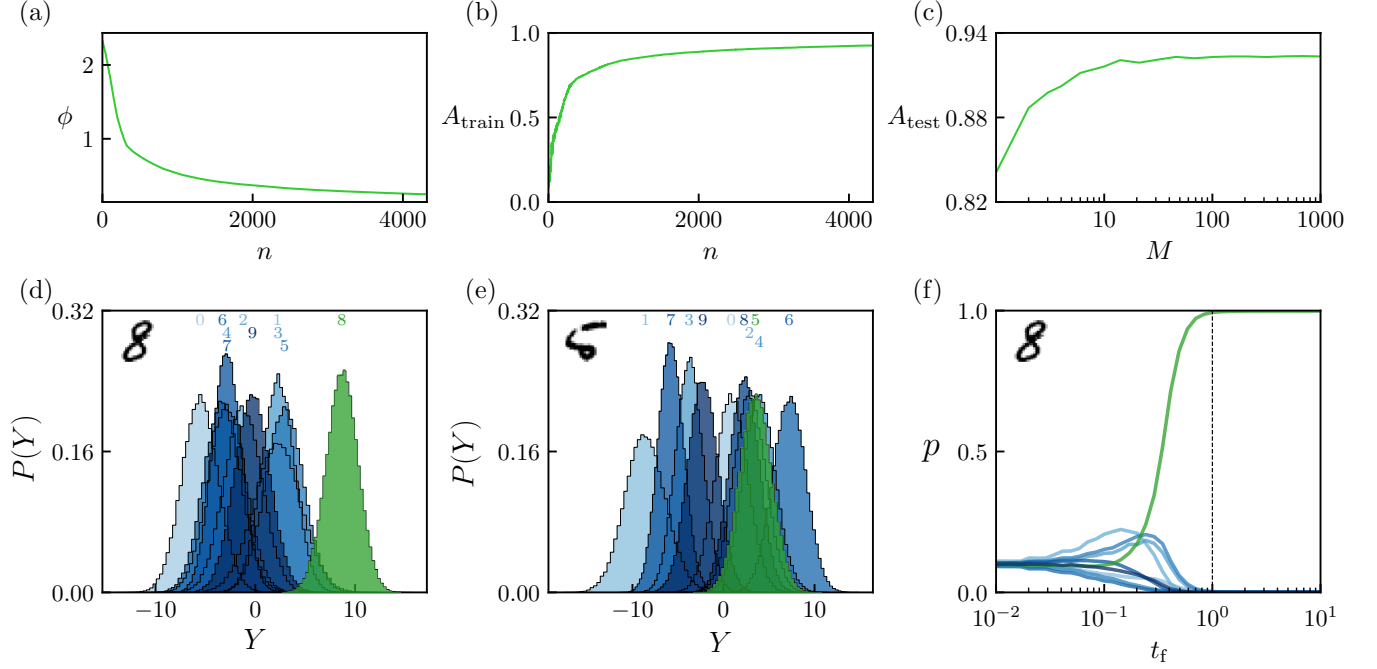


FIG. 10. Training a simulation model of a thermodynamic computer to classify MNIST. The computer, which consists of a 3-layer network of quadratic-quartic (1,0,1) neurons, is trained in reset-sampling mode, using  $M = 10^3$  samples taken at observation time  $t_f = 1$ . (a) Loss (18) as a function of evolutionary time  $n$ . (b) Training-set classification accuracy during training. (c) Test-set classification accuracy of the trained computer, as a function of the number of samples  $M$  generated by the computer (each taken at observation time  $t_f = 1$ ). (d) For a single digit, an 8, we show the probability distribution, taken over  $10^5$  samples, of the computer's per-sample class predictions, Eq. (19). The mean value (16) of each distribution, which is the value used for classification, is indicated at the top of the panel. The correct distribution is shown in green, the others in shades of blue. (e) As panel (d), but for a misclassified digit, a 5. (f) The class predictions (16) of the computer, upon being shown the indicated digit, for various observation time  $t_f$ . The computer is trained to classify the digit at an observation time  $t_f = 1$  (vertical dotted line).

shows the test-set classification accuracy of the trained computer, as a function of the number of samples  $M$  (see Eq. (11)). Training was done using  $M = 10^3$  samples per digit, but the trained computer can be run with considerably fewer samples ( $\approx 20$ ) without significant loss of accuracy. Thus while the training procedure involved the generation of more than  $10^{13}$  simulated trajectories, the trained computer (which is designed to be implemented in hardware) can afford to generate as few as 20 trajectories in order to classify individual digits with reasonable accuracy.

The test-set accuracy of the trained computer is about 93%, which is not state-of-the-art – indeed, many other methods classify MNIST with greater accuracy [38] – but the result demonstrates the ability of thermodynamic computers to do machine learning, and to carry out arbitrary nonlinear computations at specified observation times, regardless of whether or not the computer has attained equilibrium. As with conventional neural networks, better accuracy will be achieved with different computer designs and methods of training. Such incremental improvements are not the goal of the present paper. Our aim is to show proof of principle: if im-

plemented in hardware, this thermodynamic computer would be able, powered only by thermal fluctuations, to classify MNIST digits.

In Fig. 10(d) we show the output of the trained computer when presented with a single digit, an 8, which it correctly classifies. We plot the probability distribution, taken over  $10^5$  samples, of the computer's per-sample predictions

$$Y^{(C)}(\mathbf{I}) \equiv \sum_{i \in \text{outputs}} f_i^{(C)} x_i(\mathbf{I}, t_f). \quad (19)$$

The mean value of each distribution, corresponding to Eq. (16), is indicated at the top of the panel. The correct distribution is shown in green, with the others in shades of blue. Panel (e) shows similar data for a digit, a 5, that is misclassified as a 6 by the computer.

In Fig. 10(f) we plot the value of the trained computer's 10 predictions (16) upon being shown the indicated digit. The computer is trained to classify the digit at an observation time  $t_f = 1$ . In this case the computer has attained a steady-state dynamics at the specified observation time, but this is not a general phenomenon: when presented with other digits, the computer's neu-

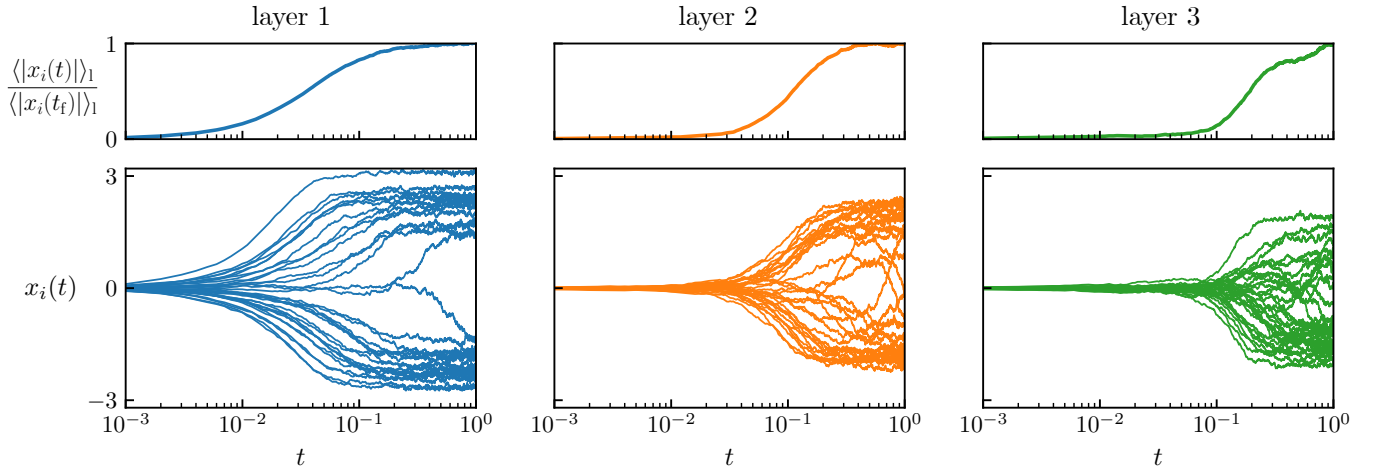


FIG. 11. Values of all neurons  $x_i$ , for a single trajectory of the 3-layer thermodynamic computer, when presented with an MNIST digit. The top panels are averaged over all neurons in the indicated layer. The computer's outputs (the layer-3 neurons) are still evolving at the observation time  $t_f = 1$ , showing that the computer operates out of equilibrium.

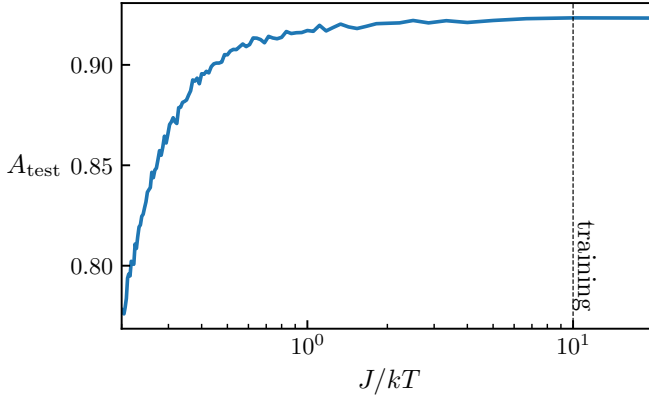


FIG. 12. MNIST test-set accuracy of the trained 3-layer thermodynamic computer at a range of energy scales (the parameters of the thermodynamic computer are held fixed, and the noise strength is varied). The computer is trained at the energy scale  $J = 10k_B T$ .

rons are still evolving at  $t_f = 1$ . In Fig. 11 we show the values of all neurons  $x_i$  for a single trajectory of the computer, as a function of time, when presented with an MNIST digit different to the one used in Fig. 10(f). The top panels of Fig. 11 are averaged over all neurons in the indicated layer. The computer's outputs are still evolving at  $t_f = 1$ , showing that the computer operates out of equilibrium.

### E. Role of noise in the thermodynamic computer

We have trained the thermodynamic computers for the cosine- and MNIST problems at an energy scale of  $J_2 = J_4 \equiv J = 10k_B T$ , which is characteristic of the energy scales of thermodynamic computing ( $J \lesssim 10k_B T$ ).

Here, noise plays a substantial role in the dynamical evolution of the device. The energy scales of classical computing are much larger ( $J \gtrsim 10^3 k_B T$ ), allowing near-deterministic operation.

The ability of the trained computer to operate at different noise scales depends on the nature of the problem it is trained for and its architecture. In Fig. 12 we show the test-set accuracy of the trained thermodynamic computer at a range of energy scales (the parameters of the thermodynamic computer are held fixed, and the noise strength is varied). The computer, trained at the energy scale  $J = 10k_B T$ , performs essentially as well when subjected to noise comparable in scale to its own energy scale ( $J = k_B T$ ). This result shows the ability of the computer to operate reliably throughout the regime characteristic of thermodynamic computing, and shows its output to be robust to small changes in noise level (which might occur if a device becomes hot during computation). For sufficiently large noise levels ( $J \lesssim k_B T$ ) the computer's performance begins to decline.

For larger energy scales,  $J \gtrsim 10k_B T$ , the computer operates reliably. This result suggests the idea of training a thermodynamic computer at larger energy scales, where noise is less important, and using the trained computer in a noisy environment. The advantage of such an approach is that, in the limit  $J/k_B T \rightarrow \infty$ , trajectories of the computer become deterministic, and training becomes much less computationally intensive. However, upon trying this strategy we found it to work in some cases but not others.

In Fig. 13(a) we show the loss associated with a thermodynamic computer trained to express the cosine function at zero noise ( $J/k_B T \rightarrow \infty$ ) and tested at a wide range of energy scales. The output values of the computer change continuously with energy scale, and so while it can tolerate the very low noise levels characteristic of classical computing, it breaks down for the larger noise levels

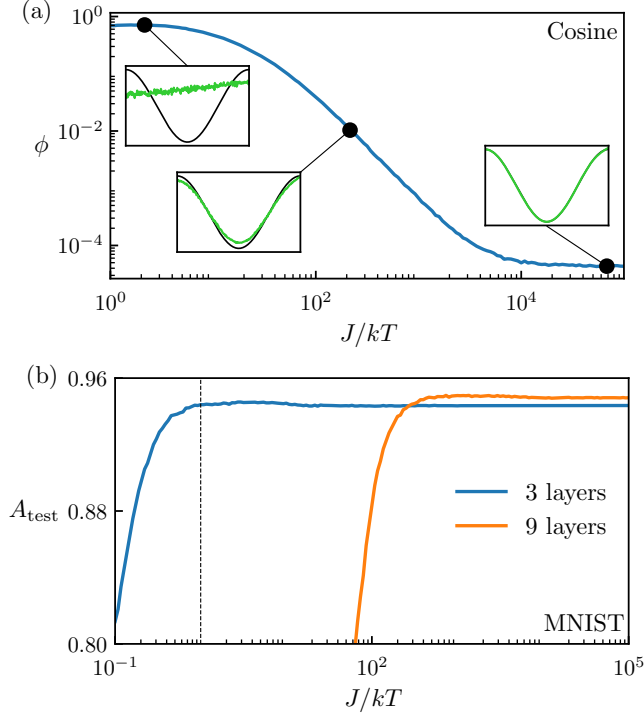


FIG. 13. (a) Loss associated with a simulated thermodynamic computer trained at zero noise to express a cosine function and operated at various finite noise levels. (b) MNIST Test-set accuracy of a 3-layer thermodynamic computer trained at zero noise to classify MNIST and operated at various finite noise levels (blue). The orange line shows the same thing for a 9-layer computer. The vertical black dashed line denotes the energy scale  $J = k_B T$ .

characteristic of thermodynamic computing. In this case, the computer must be trained in the presence of noise to operate in the presence of noise.

In Fig. 13(b) we show the MNIST test-set accuracy of a 3-layer thermodynamic computer, trained at zero noise to classify MNIST, when operated at various finite noise levels (blue). This case is different to that of panel (a); here, the accuracy changes very little as the noise is increased, even up to the noise levels characteristic of thermodynamic computing. The mean outputs of the computer change continuously with noise, and so therefore does the loss, but classification accuracy depends on the relative values of the computer’s outputs, not their absolute values, and so is less strongly affected. This is a convenient feature, because training is much less expensive in the deterministic zero-noise limit. There, we used backpropagation through time [39] on a single trajectory of the computer (for each digit), and training takes about 30 minutes on a single GPU instead of 24 hours on 96 GPUs. For some applications, therefore, it is possible to train a thermodynamic computer at zero noise, and operate it at noise levels comparable to the energy scale of the device.

The orange line in Fig. 13(b) shows the same thing

for a 9-layer thermodynamic computer trained at zero noise. This model is more accurate than the 3-layer one for small noise values, but fails more rapidly as noise is increased, and fails before we reach the large noise levels characteristic of thermodynamic computing. The reason for this failure is likely the diminishing signal-to-noise ratio, in the interior of the computer, as we move away from the input layer. This effect can be seen in the 3-layer computer shown in Fig. 11: the signal scale, and hence the signal-to-noise ratio, diminishes from input to output layers. The comparison of the two lines in Fig. 13(b) indicates that robustness to noise levels different to those seen during training is an architecture-dependent phenomenon, and suggests that the layered architecture characteristic of classical neural networks may not be an optimal design for a nonlinear thermodynamic computer.

Lastly, we note that while a thermodynamic computer trained at zero temperature may not operate reliably at finite temperature, its parameters could be used as the starting point for finite-temperature training, potentially reducing the computational expense of that process. In our finite-temperature training simulations we began with random parameters.

#### IV. CONCLUSIONS

Classical computing aims to overcome or suppress thermal fluctuations, while thermodynamic computing uses thermal fluctuations. Most thermodynamic computing algorithms proposed to date require the computer to reach thermodynamic equilibrium, and arrange for the Boltzmann distribution of the computer’s degrees of freedom to encode the outcome of a desired calculation. Although a powerful approach, one difficulty it encounters is that equilibration times for physical systems can span a broad range of timescales; a second is that not every calculation can be expressed in an obvious way by the Boltzmann distribution.

An alternative is to arrange for a thermodynamic computer to perform arbitrary nonlinear calculations at specified observation times, whether or not the computer has come to thermal equilibrium. In this paper we have presented the design for such a computer, a “thermoneural network”, and have programmed a simulation model of the computer by genetic algorithm to express a nonlinear function and to classify MNIST digits. The core of our design is a thermodynamic neuron, a fluctuating classical degree of freedom confined by a quartic potential. (In general, the confining potential need not be exactly quartic, but it must be higher-order than quadratic and thermodynamically stable; we can consider Eq. (1) to represent a Maclaurin expansion, in powers of  $x$ , of an arbitrary nonlinear thermodynamic circuit.) The neuron’s activity is a nonlinear function of its input, in and out of equilibrium, and so interacting graphs of such neurons can function as universal approximators, in and out

of equilibrium. Thermodynamic neural networks can be programmed by genetic algorithm to perform nonlinear computations analogous to those performed by conventional neural networks, at specified times, regardless of whether the system has reached equilibrium. Classical computers operate on a clock, and we have shown that thermodynamic computers can do so, too.

The thermodynamic computer design presented here uses several elements that have already been deployed in hardware. For instance, RLC circuits can encode fluctuating degrees of freedom that interact via bilinear couplings [11, 12]. However, the degrees of freedom of existing thermodynamic computers possess quadratic self-interactions, which result in linear activation functions and cannot be used to construct a universal approximator. Nonlinear inductors or capacitors might be used to induce higher-order self interactions within RLC circuits [40, 41]. Alternatively, thermodynamic computers could be built from superconducting circuits, in which case Josephson junctions can provide nonlinear inductance [22]. If such designs can be implemented, this paper shows that the resulting nonlinear computer can be programmed, e.g. by genetic algorithm. The trained

computer would evolve by thermal fluctuations to perform a specified computation at a specified observation time, whether or not the computer has attained thermodynamic equilibrium.

## ACKNOWLEDGMENTS

This work was done at the Molecular Foundry, supported by the Office of Science, Office of Basic Energy Sciences, of the U.S. Department of Energy under Contract No. DE-AC02-05CH11231. This research used resources of the National Energy Research Scientific Computing Center (NERSC), a U.S. Department of Energy Office of Science User Facility located at Lawrence Berkeley National Laboratory, operated under Contract No. DE-AC02-05CH11231. C.C. was supported by a Francqui Fellowship of the Belgian American Educational Foundation, and by the US DOE Office of Science Scientific User Facilities AI/ML project “A digital twin for spatiotemporally resolved experiments”.

- 
- [1] C. H. Bennett, *International Journal of Theoretical Physics* **21**, 905 (1982).
  - [2] R. Landauer, *Physics Today* **44**, 23 (1991).
  - [3] P. E. Ceruzzi, *A history of modern computing* (MIT Press, 2003).
  - [4] R. L. Fry, *Neurocomputing* **65**, 455 (2005).
  - [5] T. Conte, E. DeBenedictis, N. Ganesh, T. Hylton, G. E. Crooks, and P. J. Coles, arXiv preprint arXiv:1911.01968 (2019).
  - [6] T. Hylton, *Entropy* **22**, 256 (2020).
  - [7] M. P. Frank, *IEEE Spectrum* **25**, 2017 (2017).
  - [8] D. H. Wolpert, *Journal of Physics A: Mathematical and Theoretical* **52**, 193001 (2019).
  - [9] R. L. Fry, *Entropy* **19**, 107 (2017).
  - [10] G. Wimsatt, O.-P. Saira, A. B. Boyd, M. H. Matheny, S. Han, M. L. Roukes, and J. P. Crutchfield, *Physical Review Research* **3**, 033115 (2021).
  - [11] M. Aifer, K. Donatella, M. H. Gordon, S. Duffield, T. Ahle, D. Simpson, G. Crooks, and P. J. Coles, *npj Unconventional Computing* **1**, 13 (2024).
  - [12] D. Melanson, M. A. Khater, M. Aifer, K. Donatella, M. H. Gordon, T. Ahle, G. Crooks, A. J. Martinez, F. Sbahi, and P. J. Coles, arXiv preprint arXiv:2312.04836 (2023).
  - [13] F. Arceri, F. P. Landes, L. Berthier, and G. Biroli, in *Statistical and Nonlinear Physics* (Springer, 2022) pp. 229–296.
  - [14] G. Biroli and J. P. Garrahan, *The Journal of Chemical Physics* **138** (2013).
  - [15] M. F. Hagan, O. M. Elrad, and R. L. Jack, *The Journal of Chemical Physics* **135** (2011).
  - [16] S. Whitelam and R. L. Jack, *Annual review of Physical Chemistry* **66**, 143 (2015).
  - [17] S. Whitelam, arXiv preprint arXiv:2410.12211 (2024).
  - [18] S. Duffield, M. Aifer, G. Crooks, T. Ahle, and P. J. Coles, arXiv preprint arXiv:2311.12759 (2023).
  - [19] In general, the confining potential need not be exactly quartic, but it must be higher-order than quadratic and thermodynamically stable.
  - [20] G. Cybenko, *Mathematics of Control, Signals and Systems* **2**, 303 (1989).
  - [21] K. Hornik, M. Stinchcombe, and H. White, *Neural networks* **2**, 359 (1989).
  - [22] K. J. Ray and J. P. Crutchfield, *Physical Review Applied* **19**, 014049 (2023).
  - [23] J. J. Hopfield, *Proceedings of the national academy of sciences* **79**, 2554 (1982).
  - [24] D. H. Ackley, G. E. Hinton, and T. J. Sejnowski, *Cognitive science* **9**, 147 (1985).
  - [25] M. Stern, D. Hexner, J. W. Rocks, and A. J. Liu, *Physical Review X* **11**, 021045 (2021).
  - [26] P. Lipka-Bartosik, M. Perarnau-Llobet, and N. Brunner, *Science Advances* **10**, eadm8792 (2024).
  - [27] The quadratic nonlinearity also gives rise to a linear activation function out of equilibrium.
  - [28] In the purely quartic case the equilibrium activation function can be expressed analytically, in terms of the hypergeometric function.
  - [29] Y. LeCun, Y. Bengio, and G. Hinton, *nature* **521**, 436 (2015).
  - [30] J. Schmidhuber, *Neural networks* **61**, 85 (2015).
  - [31] S. R. Dubey, S. K. Singh, and B. B. Chaudhuri, *Neurocomputing* **503**, 92 (2022).
  - [32] N. Van Kampen, *Stochastic Processes in Physics and Chemistry*, 2nd ed. (North-Holland Publishing Co., Amsterdam, 1992).
  - [33] S. Dago, J. Pereda, N. Barros, S. Ciliberto, and L. Bellon, *Physical Review Letters* **126**, 170601 (2021).



- [34] S. Whitelam, V. Selin, I. Benlolo, C. Casert, and I. Tamblin, Machine Learning: Science and Technology **3**, 045026 (2022).
- [35] Y. LeCun, L. Bottou, G. B. Orr, and K.-R. Müller, in *Neural Networks: Tricks of the Trade* (1996).
- [36] L. Sabattini, A. Coriolano, C. Casert, S. Forti, E. S. Barnard, F. Beltram, M. Pontil, S. Whitelam, C. Coletti, and A. Rossi, arXiv preprint arXiv:2410.10885 (2024).
- [37] Y. LeCun, L. Bottou, Y. Bengio, and P. Haffner, Proceedings of the IEEE **86**, 2278 (1998).
- [38] Y. LeCun, C. Cortes, and C. J. Burges, “Mnist leaderboard,” <http://yann.lecun.com/exdb/mnist/> (1998).
- [39] P. J. Werbos, Proceedings of the IEEE **78**, 1550 (1990).
- [40] E. S. Kuh and I. N. Hajj, Proceedings of the IEEE **59**, 340 (1971).
- [41] L. Chua, IEEE Transactions on Circuits and Systems **27**, 1059 (1980).